

Provided for non-commercial research and education use.  
Not for reproduction, distribution or commercial use.



This article appeared in a journal published by Elsevier. The attached copy is furnished to the author for internal non-commercial research and education use, including for instruction at the authors institution and sharing with colleagues.

Other uses, including reproduction and distribution, or selling or licensing copies, or posting to personal, institutional or third party websites are prohibited.

In most cases authors are permitted to post their version of the article (e.g. in Word or Tex form) to their personal website or institutional repository. Authors requiring further information regarding Elsevier's archiving and manuscript policies are encouraged to visit:

<http://www.elsevier.com/authorsrights>



## Effects of Silicon Nanoparticles on the Transient Liquid Phase Bonding of 304 Stainless Steel

H.M. Hdz-García<sup>1)\*</sup>, A.I. Martínez<sup>2)</sup>, R. Muñoz-Arroyo<sup>1)</sup>, J.L. Acevedo-Dávila<sup>1)</sup>, F. García-Vázquez<sup>1)</sup>, F.A. Reyes-Valdes<sup>1)</sup>

1) Corporación Mexicana de Investigación en Materiales S.A. de C.V., Ciencia y Tecnología No. 790, Fracc. Saltillo 400; Saltillo, Coah. CP. 25290, Mexico

2) Centro de Investigación y de Estudios Avanzados del IPN, Carr. Mty-Saltillo km. 13, Ramos Arizpe, Coah. CP. 25900, Mexico

[Manuscript received January 19, 2013, in revised form March 20, 2013, Available online 20 November 2013]

Transient liquid phase (TLP) bonding of 304 stainless steel with nickel based filler metal, BNi-9, was performed to study the influence of silicon nanoparticles (NPs) on the mechanical and structural properties of the bonding area. It was found that silicon NPs act as a melting point depressant in the brazing process; the formation of silicon TLP induces the dissolution of elements of the metal filler and promotes a uniform distribution in the bonding area. Silicon NPs induce the development of smaller eutectic structures in the melting zone; it has been related to microhardness measurements, which are lower when the silicon NPs are used in the brazing process.

**KEY WORDS:** Brazing; Nanoparticles; Silicon; Stainless steel

### 1. Introduction

Stainless steels are essential for medical, chemical, food processing, and biotechnological applications because of their excellent corrosion resistance and hardness at room temperature. For most applications, stainless steels require bonding of components when reparation of damaged components is needed or fabrication of special geometries is required. Under certain conditions, stainless steel components are damaged because their mechanical properties are reduced or exist zones susceptible to corrosive attacks<sup>[1]</sup>. These adverse effects usually occur in bonding areas<sup>[1,2]</sup>.

There are three processes for repairing or joining metal-pieces; namely, fusion welding, diffusion bonding and brazing<sup>[2,3]</sup>. Brazing is an alternative technique for joining components made from special alloys<sup>[4–6]</sup>. However, brazed joints often contain hard and brittle intermetallic phases, which decrease the mechanical and corrosion properties of the bonding areas<sup>[3,7–9]</sup>. An alternative to prevent the formation of intermetallics is the use of transient liquid phase (TLP) bonding (also named as diffusion brazing)<sup>[3,7,10–12]</sup>, which consists of a complete isothermal

solidification of the TLP that exists temporarily during the brazing process. In the TLP bonding, the brazing metal filler should contain melting point depressants (MPD) elements such as boron, silicon and phosphorus<sup>[3,10,13,14]</sup>. MPD elements should exhibit high solubility in the base metal, which will reduce the growth of intermetallics. Currently, for development of the TLP bonding process, some alternatives have been used such as the use of nanoparticles as effective agents for retarding or avoiding the growth of intermetallic compounds<sup>[15–17]</sup>.

The aim of this work was to evaluate the effect of silicon nanoparticles (NPs) used as an additive in the TLP bonding of 304 stainless steel. It was found that the formation of TLP on cracks of 304 stainless steel promoted the following: 1) forming a liquid capable of increasing the wettability between microcracks and internal micropores, 2) improving capillary forces between the filler metals and the TLP and 3) modifying the development of deleterious intermetallic phases.

### 2. Experimental

#### 2.1. Synthesis of silicon NPs and characterization of the brazing filler metal

Silicon nanoparticles were synthesized from silicon powders (35  $\mu\text{m}$ , Aldrich) using high energy ball milling at 350 r/min for 8 h. The structure and morphology of the NPs were characterized by high resolution transmission electron microscopy (HR-TEM) in an FEI Titan microscope. The brazing filler metal selected for

\* Corresponding author. Ph.D.; E-mail addresses: [hmanuelhdz@comimsa.com](mailto:hmanuelhdz@comimsa.com) (H.M. Hdz-García), [arturo.martinez@cinvestav.edu.mx](mailto:arturo.martinez@cinvestav.edu.mx) (A.I. Martínez).

1005-0302/\$ – see front matter Copyright © 2013, The editorial office of Journal of Materials Science & Technology. Published by Elsevier Limited. All rights reserved.

<http://dx.doi.org/10.1016/j.jmst.2013.11.006>

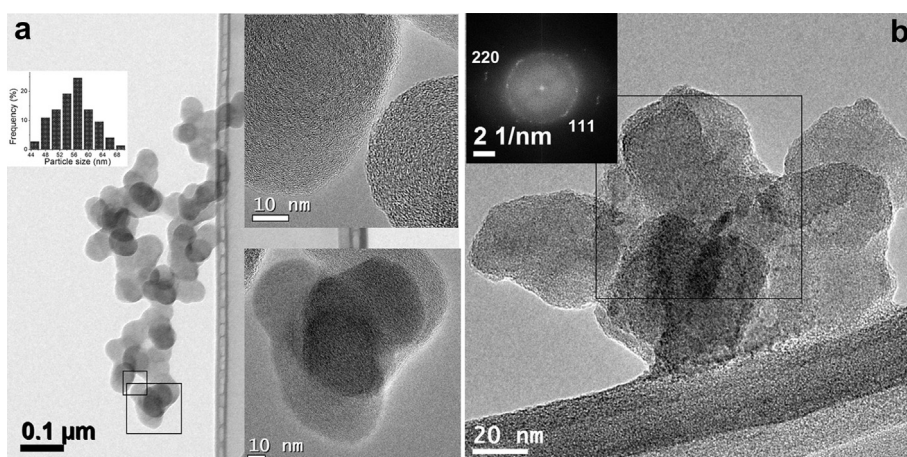


**Fig. 1** TEM images of silicon NPs obtained by high energy ball milling: (a) amorphous round shaped NPs, (b) quasi-crystalline NPs. Insets in (a) show HR-TEM images of different areas of the micrograph (right) and a histogram of particle size distribution determined by TEM (left). Inset in (b) shows the SAED pattern of the quasi-crystalline NPs.

this work was BNi-9; it was characterized by differential thermal analysis (DTA) using a Pyris Diamond Tg/DTA equipment, X-ray diffraction (XRD) in a Phillips X'Pert 3040 diffractometer and scanning electron microscopy (SEM) in a Phillips XL30 microscope.

*2.2. Generation of cracks in stainless steel and their impregnation with silicon NPs*

In order to study the brazing process and the effects of silicon NPs, cracks were generated in 304 stainless steel rods of  $\Phi 10 \text{ mm} \times 60 \text{ mm}$  by bending them with a mechanical testing machine; these fractures were inspected by SEM. For the impregnation of the cracks with NPs, a mixture of 0.5 g of silicon NPs in 200 ml of ethanol was sonicated for 1 h. Subsequently, the steel with cracks was placed in the dispersed silicon NPs and sonicated for 30 min. This sonicating time promotes the diffusion of silicon NPs inside the microcracks.

*2.3. Brazing of cracked 304 stainless steel*

In order to evaluate the effect of silicon NPs in the brazing process of the stainless steel, the BNi-9 filler metal (Nicrobraz, Wall Colmonoy) was used in the cracked rods with and without

silicon NPs impregnation. The brazing process was conducted in a sealed tube furnace under an Ar gas flow of 0.1 L/min at the brazing temperature of 1200 °C for 10, 20, 30 and 60 min; the heating and cooling rates were fixed at 10 °C/min. Additionally, in order to determine the reactivity of the silicon NPs on the cracked stainless steel, the impregnated cracks were subjected to the same conditions described above, at 1000 and 1200 °C. The resulting samples were characterized by SEM and optical microscopy. The microhardness measurements were performed in a Vickers/Knoop hardness tester by Wilson Instruments Tukon 2100B using a load of 500 g with a pyramidal indenter. 15 microhardness measurements were realized in each zone, namely melting zone, isothermal zone and base metal.

**3. Results and Discussion**

*3.1. Characterization of silicon NP and BNi-9 filler metal*

The morphology and structure of the silicon NP were studied by HR-TEM. Fig. 1 shows TEM micrographs of the silicon NP synthesized by ball milling. It was found that the sample consists of two kinds of nanoparticles. Fig. 1(a) displays a bright field image of one kind of NPs that were found in the sample. The round shaped NPs with sizes among 45–70 nm can be

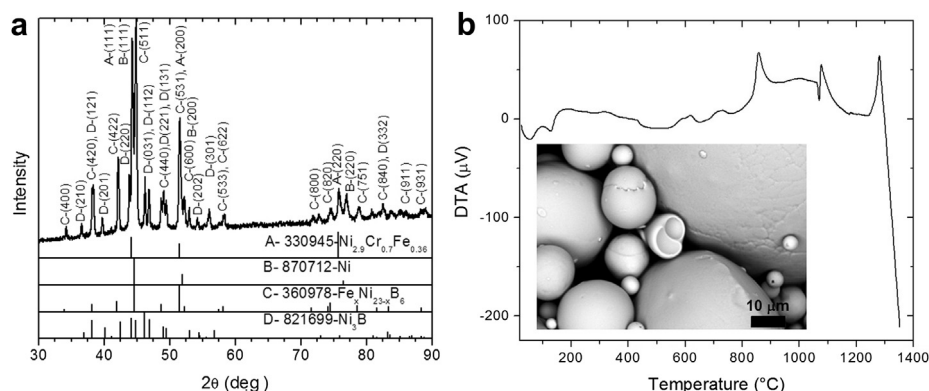


**Fig. 2** Analyses of the BNi-9 filler metal: (a) XRD pattern, (b) DTA; the inset showing a SEM image.

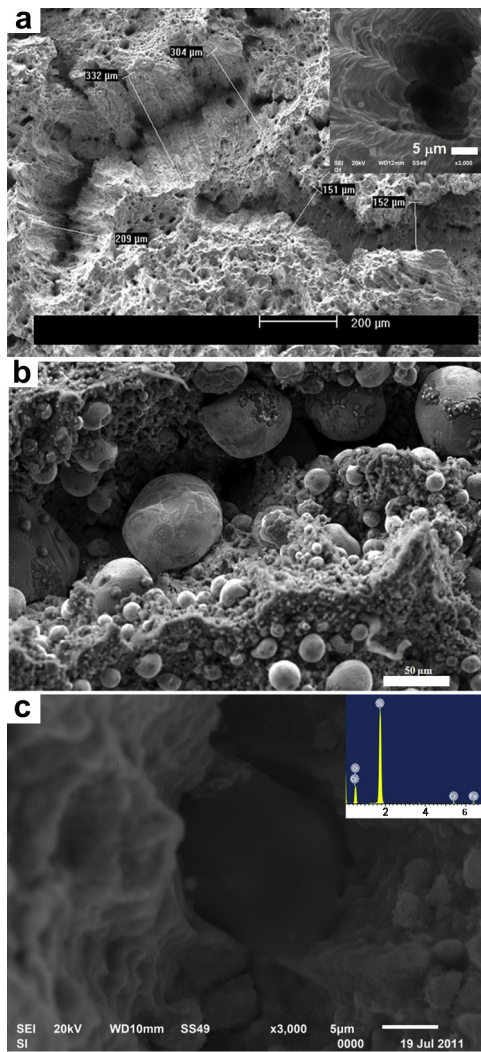


**Fig. 3** SEM micrographs of the fractured surface of 304 stainless steel: (a) without silicon NPs, the inset shows a zoom of a micropore, (b) with silicon NPs impregnation process after an annealing process at 1200 °C for 60 min, (c) interaction of silicon NPs with the stainless steel fractured surfaces after an annealing process at 1000 °C for 20 min.

appreciated in the sample. The insets shown in Fig. 1(a) display HR-TEM images, in both insets it can be appreciated that no crystal arrangements are present in the silicon NPs. Fig. 1(b) shows an HR-TEM image where silicon NPs are observed with non-defined shape; in the inset a fast Fourier transform of the

squared area is shown, here the spots are indexed to the cubic structure of silicon. As a conclusion, by TEM analyses, the sample obtained by high energy ball milling is composed by both amorphous round shaped NPs and non-defined shape quasi-crystalline silicon NPs.

The characterization of the BNi-9 filler metal by XRD, SEM and DTA yielded important information that is necessary for understanding the role of the silicon NPs on the stainless steel brazing process. The composition of BNi-9 is as follows (in wt%): Cr 15, B 3.6, P 0.02 and Ni (remainder). Fig. 2 shows the XRD, DTA and SEM analyses of the BNi-9 filler metal. The indexation of the XRD pattern revealed that the filler metal is predominantly composed by polycrystalline cubic phases such as nickel,  $\text{Ni}_{2.9}\text{Cr}_{0.7}\text{Fe}_{0.36}$ ,  $\text{Fe}_x\text{Ni}_{23-x}\text{B}_6$ , and the orthorhombic  $\text{Ni}_3\text{B}$  phase. The DTA analysis shown in Fig. 2(b) displays a small endothermic peak at 1080 °C, which is assigned to the melting point of the BNi-9 metal filler. The SEM micrograph shown as an inset in Fig. 2(b), displays round shaped particles with wide size dispersion. It can be observed that the particles size runs from around of 2 μm to several tens of micrometer.

### 3.2. Effect of silicon NPs on the brazing process

As a preliminary step to the brazing process, the behavior of silicon NPs on the 304 stainless steel fractures was evaluated by SEM. Fig. 3 shows SEM micrographs of the fractured surface of 304 stainless steel with and without the silicon NPs impregnation process. In Fig. 3(a) microcracks of ~150 μm and ~300 μm can be observed on the fractured surface. Fig. 3(b) shows the result of the interaction of silicon NPs with the stainless steel fracture surface after an annealing process at 1200 °C for 60 min. The growth of round shaped silicon particles on the stainless steel fractured surface can be seen. An important observation is that silicon particles grown inside the microcracks are greater than those grown outside of them. The generation of greater spheres inside the microcracks may be due to the coalescence of smaller particles that fall in the cracks. In fact, it can be observed in the SEM micrograph that microspheres inside the cracks are of ~65 μm in size, and they are composed of smaller particles of around 5 μm. Fig. 3(c) shows the result of the interaction of silicon NPs with the stainless steel fractured surfaces after an annealing process at 1000 °C for 20 min. It can be observed a bead in the lower part of the crack; the composition of the bead is near pure silicon (see the EDX spectrum in the inset). The formation of the bead inside the pore can be inferred from the formation of a liquid silicon phase, however, the melting point of bulk silicon is around 1400 °C. The formation of liquid silicon at lower temperatures is possible, because it is well known that the melting point of nanoparticles is much lower than the melting

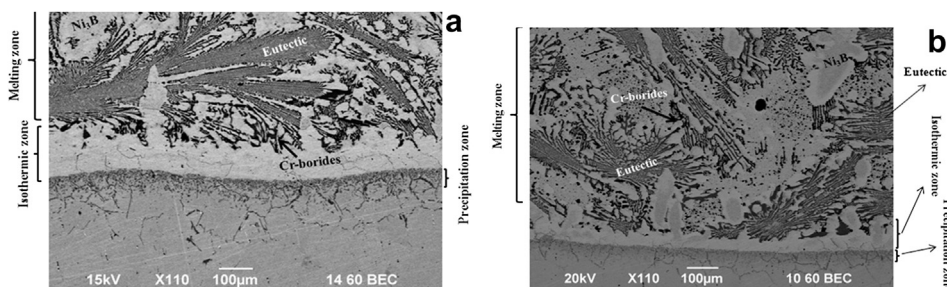


**Fig. 4** Areas joined by the brazing process realized at 1200 °C for 60 min with the BNi-9 metal filler, without (a) and with (b) silicon NPs impregnation.

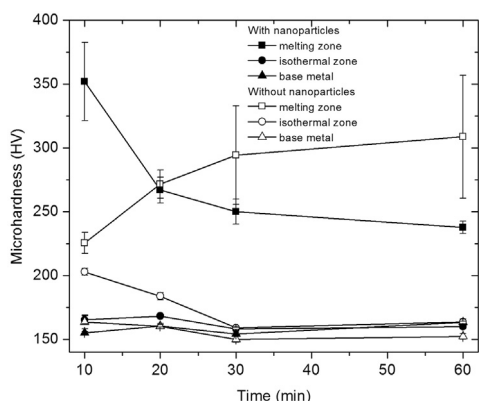


**Fig. 5** Microhardness measured in the bonding areas as a function of the brazing time, with and without silicon NPs impregnation.

temperature of bulk silicon<sup>[18]</sup>; for example, silicon NPs with a size of  $\sim 20$  nm start melting at around  $727$  °C<sup>[18]</sup>. As a conclusion, the use of silicon NPs will promote the formation of a TLP at lower temperatures; as a consequence, it will promote the dissolution of other species in the brazing process.

The areas joined by the brazing process realized at  $1200$  °C for 60 min with the BNi-9 metal filler are shown in Fig. 4. The bonding areas consist of three different zones, which are the melting zone (MZ), the isothermally solidified zone (ISZ) and the precipitation zone (PZ). Fig. 4(a) shows a SEM image of the bonding region realized without silicon NPs impregnation; it can be observed that the MZ includes large lamellar-arborescent morphology structures, which correspond to Ni–Cr–Fe eutectic, and small non-uniform structures, whose composition correspond to Cr-borides. In contrast, it can be observed in Fig. 4(b) that the silicon NPs used in the brazing process promote a change in the size, morphology and distribution of the structures in the MZ. When silicon NPs are used, the lamellar eutectic structures are smaller, and the Cr-borides are uniformly distributed in the MZ. On the other hand, the ISZ in Fig. 4(b) is narrower than that shown in Fig. 4(a) because the isothermal solidification of liquid interlayer is enriched with silicon, which improves fluidity, and modifies the solidification rate<sup>[9,13]</sup>. It is noteworthy that the presence of silicon NPs in the brazing process promotes the TLP bonding, modifies the growth of Ni–Cr–Fe structures and the distribution of borides.

In order to evaluate the effect of silicon NPs on the mechanical properties in the brazing process, the microhardness was measured in the bonding areas as a function of the brazing time. It can be seen in Fig. 5 that in the MZ, microhardness increases in the samples without the addition of silicon NPs as eutectics are greater with the brazing time. It can be observed in the microhardness vs. time graph that in the MZ the error bars are very large due to the microstructure observed in this zone (see Fig. 4(a)). In contrast, when silicon NPs were used, the microhardness diminishes with the brazing time, it is because the use of silicon diminishes the size of eutectic structures and promotes a high distribution of boron in the MZ. The formation of large eutectic structures in the bonding zone generates hard and brittle brazed joints that will possess non-adequate mechanical and

corrosion resistance properties<sup>[15]</sup>. It is noteworthy that the microhardness in other zones of the bonding areas does not present significant variations when silicon NPs were used. The microhardness diminishing promoted by silicon NPs is a beneficial characteristic in the bonding zone because it will be less brittle.

#### 4. Conclusion

The main role of silicon NPs is to act as a melting point depressant in the brazing process. The use of silicon NPs promotes the formation of TLP at low temperatures ( $\sim 1000$  °C); this phase induces the dissolution of elements of the metal filler and promotes a uniform distribution in the bonding area. SEM observations of the bonding zones reveal that silicon NPs induce the development of smaller eutectic structures in the melting zone; it has been related to microhardness measurements, which are lower when the silicon NPs are used in the brazing process.

#### Acknowledgment

This work was supported by the National Council of Science and Technology (CONACYT).

#### REFERENCES

- [1] B. Holmberg, *Stainless Steels—Their Properties and Their Suitability for Welding*, AvestaPolarit Stainless Brochure 9473:2, Avesta, 2002.
- [2] P.J. Cuna, *The Welding of Stainless Steels*, Euro Inox, Luxembourg, 2007.
- [3] V. Jalilvand, H. Omidvar, H.R. Shakeri, M.R. Rahimpour, *Mater. Charact.* 75 (2013) 20–28.
- [4] M. Abdelfatah, O.A. Ojo, *Mater. Sci. Technol.* 25 (2009) 61–67.
- [5] R.M.D. Nascimento, A.E. Martinelli, A.J.D.A. Buschinelli, U. Reigen, J. Remmel, *J. Mater. Sci.* 40 (2005) 4549–4556.
- [6] A. Ghoneim, O.A. Ojo, *Mater. Charact.* 62 (2011) 1–7.
- [7] G.O. Cook, I.I.I. Carl, *J. Mater. Sci.* 46 (2011) 5305–5323.
- [8] J.T. Stover, *Review of the State of the Art of High-temperature Brazing for Combustion Turbine Components*, ERPI, Palo Alto, CA, 2003, p. 1005029.
- [9] M.A. Arafin, M. Medraj, D.P. Turner, P. Bocher, *Mater. Sci. Eng. A* 447 (2007) 125–133.
- [10] M. Mosallae, A. Ekrami, K. Ohsasa, K. Matsuura, *Metall. Mater. Trans. A* 39 (2008) 2389–2402.
- [11] O.A. Idowu, O.A. Ojo, M.C. Chaturvedi, *Metall. Mater. Trans. A* 37 (2005) 2787–2796.
- [12] M. Pouranvari, A. Ekrami, A.H. Kokabi, *J. Alloy. Compd.* 469 (2009) 270–275.
- [13] N.P. Wikstrom, A.T. Egbewande, O.A. Ojo, *J. Alloy. Compd.* 460 (2008) 379–385.
- [14] N.R. Philips, C.G. Levi, A.G. Evans, *Metall. Mater. Trans. A* 39 (2007) 142–149.
- [15] S.Y. Chang, C.C. Jain, T.H. Chuang, L.P. Feng, L.C. Tsao, *Mater. Des.* 32 (2011) 4720–4727.
- [16] R. Eluri, B.K. Paul, *Mater. Des.* 36 (2012) 13–23.
- [17] R. Eluri, B. Paul, *J. Manuf. Process.* 14 (2012) 471–477.
- [18] G. Schiering, R. Theissmann, H. Wiggers, D. Sudfeld, A. Ebbens, D. Franke, V.T. Witusiewicz, M. Apel, *J. Appl. Phys.* 103 (2008) 084305.

# InCites™ Journal Citation Reports®



THOMSON REUTERS™

[Home](#)

[Journal Profile](#)



## JOURNAL OF MATERIALS SCIENCE & TECHNOLOGY

ISSN: 1005-0302

JOURNAL MATER SCI TECHNOL  
72 WENHUA RD, SHENYANG 110015, PEOPLES R CHINA  
**CHINA MAINLAND**

[Go to Journal Table of Contents](#)

[Go to Ulrich's](#)

### Titles

ISO: J. Mater. Sci. Technol.  
JCR Abbrev: J MATER SCI TECHNOL

### Categories

MATERIALS SCIENCE,  
MULTIDISCIPLINARY - SCIE;  
METALLURGY & METALLURGICAL  
ENGINEERING - SCIE;

### Languages

ENGLISH

6 Issues/Year;

### Key Indicators

Year ▾	Total Cites <a href="#">Graph</a>	Journal Impact Factor <a href="#">Graph</a>	Impact Factor Without Journal Self Cites <a href="#">Graph</a>	5 Year Impact Factor <a href="#">Graph</a>	Immediacy Index <a href="#">Graph</a>	Citable Items <a href="#">Graph</a>	Cited Half-Life <a href="#">Graph</a>	Citing Half-Life <a href="#">Graph</a>	Eigenfactor Score <a href="#">Graph</a>	Article Influence Score <a href="#">Graph</a>
2013	2,091	1.610	1.270	1.420	0.243	189	4.3	7.6	0.00542	0.362
2012	1,494	1.198	1.010	1.018	0.116	173	4.9	8.3	0.00432	0.283
2011	1,213	0.738	0.650	0.867	0.116	189	4.8	8.2	0.00417	0.267
2010	1,025	0.759	0.706	0.740	0.058	190	4.6	8.0	0.00411	0.238